Supporting Information

A closer look at molecular mechanisms underlying inhibition of *S*-adenosyl-L-homocysteine hydrolase by transition metal cations

Magdalena Gawel,[a] Piotr H. Malecki, [a] Joanna Sliwiak,[a] Marlena Stepniewska,[a] Barbara Imiolczyk,[a] Justyna Czyrko-Horczak,[b] Dorota Jakubczyk,[a], Łukasz Marczak,[a] Marta Plonska-Brzezinska,[*c] and Krzysztof Brzezinski[*a]

[a] Institute of Bioorganic Chemistry, Polish Academy of Sciences, Noskowskiego 12/14, 61-704 Poznan, Poland. E-mail:k.brzezinski@ibch.poznan.pl
[b] Provincial Sanitary-Epidemiological Station in Bialystok, Legionowa 8, 15-099 Bialystok.
[c] Faculty of Pharmacy with the Division of Laboratory Medicine, Medical University of Bialystok, Mickiewicza 2A, 15-222 Bialystok, Poland. E-mail: marta.plonska-brzezinska@umb.edu.pl

Table of Contents

S1 Material and Methods

S1.1 Protein production and purification

The production and purification of the active form of PaSAHase containing NAD^+ cofactor were performed as described previously[1] in the presence of a potent Zn^{2+} ions chelator, tetrakis-(2-pyridylmethyl)ethylenediamine (TPEN). PaSAHase-NADH variant of the protein was obtained similarly to the active form of the enzyme. The only difference was the incubation step of the apo form of PaSAHase with NADH instead of NAD^+.

S1.2 Assays for PaSAHase inhibition by transition metal cations

The inhibition studies were performed spectrophotometrically and the rate of L-homocysteine production was measured by monitoring its reaction at 293 K with 5,5-dithio-bis-(2-nitrobenzoic acid (DNTB)[2], as described previously.[1] At initial stages of the study, PaSAHase (0.35 μM) and adenosine deaminase (6U) in a buffer containing 100 mM KCl and 25 mM Tris·HCl pH 8.0 were incubated one hour with Zn^{2+}, Cu^{2+}, Cd^{2+}, Co^{2+}, Ni^{2+}, Mn^{2+}, Fe^{2+} and Fe^{3+} (as chlorides) at three difference concentrations, namely 1, 10 and 100 μM. Next, the reaction was started by adding SAH (100 μM) and (DNTB) (100 μM). As a negative control, the reaction was used without adding any transition metal cations. After 5 minutes of incubation, an absorbance was monitored at 412 nm using a U-3900H spectrophotometer (Hitachi). Based on these experiments, we revealed that Mn^{2+} and Fe^{3+} did not affect PaSAHase's activity. Two cations, namely Ni^{2+} and Fe^{2+}, similarly inhibited PaSAHase. However, at this point we skipped further biochemical experiments with Fe^{2+} ions, as rapid protein precipitation was observed. Two other cations, Hg^{2+} and Cu^{+} were not tested in the above experiments. Their influence on the enzyme activity was analyzed in the final measurements.

In the final measurements, the PaSAHase (0.35 μM) and adenosine deaminase (6U) in a buffer containing 100 mM KCl and 25 mM HEPES·KOH pH 7.5 were incubated for one hour with Hg^{2+}, Cd^{2+}, Cu^{2+}or Ni^{2+} (as chlorides) or Cu^{+} (as tetrakis(acetonitrile)copper(I) tetrafluoroborate to avoid fast disproportionation of Cu^{+} ions in a solution to Cu^{2+} and Cu) at different concentrations, ranging from 1 nM to 10 mM. Next, the reaction was started by adding SAH (100 μM) and (DNTB) (100 μM) and monitored for 1 minute at 412 nm using Hidex Sense Plate. A 100% activity was assigned to the sample without adding any transition metal cation.

All measurements were performed in two replicates. The data were analyzed using the *GraFit* 7.0 (Erithacus Software) to obtain the IC_{50} values. The *IC_{50}-to-K_i converter*[3] was applied to calculate the inhibition constant (K_i) for these ions using the noncompetitive inhibition model.

S1.3 Isothermal titration calorimetry

Microcalorimetric titrations of both open and closed forms of PaSAHase with different divalent cations were conducted using MicorCal iTC 200 and MicroCal PEAQ-ITC calorimeters (Malvern). Prior to the titrations, protein aliquot stored at 193 K was dialyzed against a buffer containing 50 mM Tris pH 7.5 and 100 mM KCl (for adenosine-free, open form of the enzyme) or in the same buffer with the addition of 600 µM of adenosine (for the adenosine-bound, closed form of the enzyme). Chlorides (Cd^{2+}, Hg^{2+}, Zn^{2+}, Co^{2+}, Cu^{2+}, Ni^{2+}) were dissolved in the dialysis buffers to the final concentration of 1-2 mM. The metal cation ligand was injected in 19 aliquots of 2 µL into the cell with the protein at 80-100 µM concentration (determined at 280 nm). Measurements were conducted at 293 K. Reference power was set to 5. A stirring speed of 750 rpm and spacing of 150 s was used. Data were performed in duplicate. Raw ITC data were analyzed with the *Origin* 7.0 software (Origin-Lab) to obtain thermodynamic parameters like stoichiometry (*N*), dissociation constant (K_d) and the changes in the enthalpy (ΔH) and entropy. *One set of binding sites* or *Two sets of binding sites* models (in the case of Hg^{2+} titrations to the open form of the protein) were fitted to the data.

S1.4 Thermal shift assays

Thermal shift assays were performed using the CFX96 Touch Real-Time PCR Detection System. Each 25 µL solution containing 100 mM HEPES·KOH pH 7.5, 7.5 µM PaSAHase (without addition of adenosine for the open form of the enzyme or incubated overnight with 100 uM adenosine for the closed form of the enzyme), 70 µM tetrakis(acetonitrile)copper(I) tetrafluoroborate or $MeCl_2$ (where M^{2+} corresponds to Cd^{2+}, Hg^{2+}, Zn^{2+}, Co^{2+}, Cu^{2+}, Ni^{2+}), 2.5 µL SYPRO™ Orange Protein Gel Stain (5000X in DMSO) diluted 1:100 in water was dispensed on 96-well PCR plate and incubated at 277 K for two hours. The negative controls contained no SYPRO® Orange dye or no protein, respectively. Next, melting curves were recorded for each 0.5 K temperature increment ranging from 277 to 368 K in 30 minutes.[4] Melting points were calculated by plotting the first derivative of the fluorescence emission as a function of temperature (−d(RFU)/dT).

S1.5 Analysis of PaSAHase-Cu^{2+} interactions

Fluorescence analysis of PaSAHase-Cu^{2+} interactions

The studies were performed at 293 K, and the reduced form of the cofactor (NADH) was monitored spectrofluorometrically by excitation at 340 nm and emission measurement at 460 nm. All experiments were conducted for 15 μM PaSAHase (NAD^+ or NADH variant) in a buffer containing 100 mM KCl and 25 mM HEPES·KOH pH 7.5. In the first experiment, the NADH formation was initiated by adding 2'-deoxyadenosine (2'-dAdo) to the final concentration of 5 mM to the solution containing the PaSAHase-NAD^+ variant. In the second experiment, fluorescence was monitored for the solution containing the PaSAHase-NADH variant for around two minutes. Afterward, $CuSO_4$ was added to the final concentration of 45 μM. In the third experiment, fluorescence was monitored for the mixture containing the PaSAHase-NAD^+ variant supplemented with 45 μM $CuSO_4$ and 5 mM 2'-dAdo. For all reactions, the fluorescence was monitored for 3000 seconds.

Setting up the reactions for mass spectrometry analysis

The frozen protein sample was dialyzed against 100 mM potassium acetate pH 7.5 supplemented with 70 μM TPEN for 2h, then the buffer was exchanged to 100 mM potassium acetate pH 7.5 without any addition for 1h. Assays for enzyme activity and inhibition in the hydrolytic directions were performed in 1.5 mL volume in a solution containing 100 mM potassium acetate pH 7.5, 10 μM PaSAHase, 400 μM SAH. For the inhibition study performed in the same solution, 100 μM $CuSO_4$ was added to the enzyme and incubated for 30 minutes before adding the substrate. All reactions were performed for 15 minutes at 293 K and flash-frozen in liquid nitrogen.

Mass spectrometry analysis of SAHase products

Samples from the reactions described above were prepared by dilution until the final concentration of 200uM with LCMS grade acetonitrile centrifuged, and the supernatants were filtered through a 0.22 μm filter. The samples were analyzed using an LC/MS system comprising a Dionex RLSC 3000 UPLC system (Thermo Scientific, Bremen, Germany) combined with a Q-ToF mass spectrometer, model TIMS Tof Pro (Bruker Daltonics, Bremen, Germany). Analyses were performed using the Supelco Ascentis RP18 column (2.1 ×100 mm, 3 μm).

Chromatographic separation was performed at a flow rate of 0.5 mL/min using mixtures of the following two solvents: A (99.9% H2O, 0.1% formic acid (v/v)) and B (99.9% acetonitrile, 0.1% formic acid (v/v)). The elution steps were as follows: 0–5 min linear gradient to 40% B, from 5 to 10 gradient to 90%, isocratic elution up to 15 min, followed by recovery of initial conditions for next 5 min.

The TIMS Tof Pro mass spectrometer consisted of ESI operating in positive ion mode at - 4.5 kV, nebulization with nitrogen at 1.6 bar and a dry gas flow of 8.0 L/min at a temperature of 220°C. The system was calibrated externally using a calibration mixture containing sodium formate clusters. Additional internal calibrations were performed for every run by injecting the calibration mixture using a divert valve during LC separation. Calibrations were performed using the HPC quadratic algorithm. These calibrations yielded an accuracy of less than 5 ppm. MS/MS spectra were acquired in a data-dependent mode based on ions chosen from the MS survey scan. The collision energy was dependent on the molecular masses of the compounds and was set between 15 and 25 eV. The instrument operated using the program otofControl version 6.2 and data were analyzed using the *DataAnalysis* version 6.0 package, which Bruker Daltonics supplied.

S1.6 Crystallization and data collection

Protein solution in a buffer containing 100 mM KCl, 25 mM HEPES·KOH pH 7.5, and 1 mM TCEP·HCl was incubated overnight with 2 mM of adenosine at 277 K. Crystallization drops were mixed from 2 µL of the protein solution (10 mg·mL^{-1} measured spectrophotometrically at 280 nm) and 2 µL of one of the two selected Morpheus screen condition (MDL): D9 condition containing 0.02 M 1,6-hexanediol, 0.02 M 1-butanol, 0.02 M (RS)-1,2-propanediol, 0.02 M 2-propanol, 0.02 M 1,4-butanediol, 0.02 M 1,3-propanediol, 10% w/v PEG 20 000, 20% v/v PEG MME 550, 0.1 M bicine/Trizma base pH 8.5 or Morpheus C8 condition containing 0.03 M sodium fluoride, 0.03 M sodium bromide, 0.03 M sodium iodide, 12.5% w/v PEG 1000, 12.5% w/v PEG 3350, 12.5% v/v MPD, 0.1 M MOPS/HEPES-Na pH 7.5. Diffraction-quality crystals were grown within a few days at 292 K using the hanging-drop vapor-diffusion method. The crystals were soaked in the crystallization condition D9 supplemented with Zn^{2+}, Co^{2+}, Cd^{2+}, Hg^{2+}, Ni^{2+} and Cu^{2+}, with the final concentration for the metal cation ranging from 20 to 40mM (Zn^{2+}: 25 mM, 11 minutes; Co^{2+} 40 mM, 7 min; Hg^{2+} 20 mM, 2 minutes; Cd^{2+} 20 mM, 6 minutes; Ni^{2+}: 40 mM, 15 minutes; Cu^{2+}: 15 mM, 10 minutes) and condition C8

supplemented with tetrakis(acetonitrile)copper(I) tetrafluoroborate (20 mM, 10 minutes). Crystals were soaked for 2 to 15 minutes, depending on the visual assessment of the crystal quality, as they were disintegrating. Crystals were fished directly from the mother liquor and vitrified in liquid nitrogen before X-ray data collection. The X-ray diffraction data were measured at PETRAIII EMBL beamline P13[5] and Rigaku PhotonJet-R home source. Raw diffraction images for all the structures have been deposited in the Macromolecular Xtallography Raw Data Repository (https://mxrdr.icm.edu.pl) with DOI numbers 10.18150/5AWAJZ for 7ZD0, 10.18150/UROCDW for 7ZD1, 10.18150/K6NJZX for 7ZD2, 10.18150/AFE7CL for 7ZD3 and 10.18150/CT5OD5 for 7ZD4.The diffraction images were indexed and integrated with the XDS package[6] and CrysAlisPro software (Rigaku). The intensity data were scaled in XDS. The final data set statistics are characterized in Supplementary Table S3.

S1.7 Structure solution, refinement and validation

The crystal structure of PaSAHase in the 3'-dAdo/K+ complex was solved by molecular replacement, as implemented in the program *PHASER*[7] from the *CCP4* suite[8] using a PaSAHase model (PDB entry 6F3M).[1] For all datasets, the correct solution was found in space group *C*2 with four subunits in the asymmetric unit, corresponding to the active homotetramer of PaSAHase. Isotropic stereochemically-restrained structure-factor refinement was carried out in *REFMAC5*[9] with maximum-likelihood targets and with the inclusion of three TLS[10], as suggested by the *TLSMD* server[11,12]. The ligands were identified without ambiguity in mF_o-DF_c omit electron density maps phased with the contribution of the protein atoms only. The occupancy of the ions was adjusted manually to satisfy electron density maps and ADP parameters. The *COOT* program[13] was used for manual modelling in electron density maps. The stereochemical quality of the models was assessed using the *wwPDB* validation pipeline.[14] Final refinement statistics for all four crystal structures are reported in Supplementary Table S3. The atomic coordinates and structure factors have been deposited in the Protein Data Bank with the accession codes 7ZD0 (PaSAHase-NAD^+-Ado-Cd^{2+} complex), 7ZD1 ((PaSAHase-NAD^+-Ado-Hg^{2+} complex), 7ZD2 ((PaSAHase-NAD^+-Ado-Co^{2+} complex), 7ZD3 (PaSAHase-NAD^+-Ado-Zn^{2+} complex) and 7ZD4 (PaSAHase-NAD^+-Ado complex incubated with Cu^+ ions).

S1.8 Data availability

The data supporting this article have been included as part of the Supplementary Information. The atomic coordinates and structure factors can be accessed at PDB. Raw diffraction images have been deposited in the MX-RD Repository**.**

Supplementary Tables

Table S1. Enzyme inhibition parameters characterising the influence of transition metal cations on PaSAHase. The obtained values are averages of two replicates and ± correspond to the standard error of the mean values.

Cation	IC_{50} [μM]	K_i [nM]
Cd^{2+}	0.18 ± 0.01	5.00 ± 0.28
Zn^{2+}	0.26 ± 0.01	85.00 ± 3.27
Hg^{2+}	0.36 ± 0.01	185.00 ± 5.14
Cu^{2+}	0.577 ± 0.001	279.00 ± 0.48
Cu^{+}	0.72 ± 0.01	545.00 ± 7.57
Co^{2+}	63.81 ± 3.98	$(63.635 \pm 3.969)\times10^3$
Ni^{2+}	472.95 ± 38.53	$(472.775 \pm 38.516)\times10^3$

Table S2. Thermodynamic parameters of PaSAHase-M^{2+} binding in the absence (no Ado, corresponding to the ligand-free PaSAHase in the open form) or presence of 600 μM Ado (corresponding to PaSAHase-Ado complex in the closed conformation). The parameters calculated from curve fitting are given with standard deviations as follows: stoichiometry (*N*), dissociation constant (K_d) and changes in enthalpy (ΔH) and entropy (ΔS).

ion	PaSAHase sample	*N*	K_d [μM]	ΔH [cal/mol]	ΔS [cal/mol/deg]
Cd^{2+}	no Ado	0.77 ± 0.01	2.6 ± 0.3	-8081 ± 127	-2
	600 μM Ado	0.70 ± 0.01	0.32 ± 0.11	-3216 ± 104	18.7
Hg^{2+}	no Ado*	N_1= 0.90 ± 0.06 N_2= 1.61 ± 0.05	K_{d1} = 0.21 ± 0.08 K_{d2} = 6.0 ± 0.7	ΔH_1= - 11000 ± 286 ΔH_2 = - 8037 ± 390	ΔS_1= -6.9 ΔS_2= -3.5
	600 μM Ado	1.54 ± 0.11	8.8 ± 3.3	-9395 ± 919	-8.9
Zn^{2+}	no Ado	0.82 ± 0.09	20 ± 4	-6057 ± 841	0.8
	600 μM Ado	1.20 ± 0.05	21 ± 3	-2790 ± 164	11.9
Co^{2+}	no Ado	0.92 ± 0.08	53 ± 7	-3249 ± 383	8.5
	600 μM Ado	-	-	-	-
Ni^{2+}	no Ado	1.14 ± 0.08	83 ± 11	-5079 ± 498	1.4
	600 μM Ado	0.94 ± 0.17	84 ± 7	-4020± 923	4.9
Cu^{2+}	no Ado	-	-	-	-
	600 μM Ado	-	-	-	-

*Parameters obtained in fitting the Hg^{2+}-PaSAHase (open) titration curve with the model of *Two sets of binding sites*.

Table S3. Crystallographic data and refinement statistics for PaSAHase-Ado-M^{2+} complexes.

	PaSAHase(Hg^{2+})	**PaSAHase(Cd^{2+})**	**PaSAHase(Co^{2+})**	**PaSAHase(Cu^{+})**	**PaSAHase(Zn^{2+})**
Data collection and processing statistics					
X-ray source	EMBL/ PETRA III P13	EMBL/PETRA III P13	Rigaku PhotonJet-R	Rigaku PhotonJet-R	Rigaku PhotonJet-R
Wavelength (Å)	0.976	1.700	1.541	1.541	1.541
Resolution range (Å)	52.74-1.56 (1.62-1.56)*	43.95-1.87 (1.94-1.87)	28.69-2.16 (2.24-2.16)	34.97-2.14 (2.22-2.14)	28.20-1.90 (1.97-1.90)
Space group	*C*2	*C*2	*C*2	*C*2	*C*2
Unit-cell parameters (Å, °)					
a	177.4	177.0	177.1	175.7	177.2
b	134.2	134.2	134.2	133.6	134.1
c	108.7	108.9	109.6	107.0	108.5
β	105.9	106.1	106.1	105.2	105.7
Total reflections	2336682 (213530)	1605585 (64672)	405123 (41224)	485035 (21044)	702904 (33951)
Unique reflections	344105 (33885)	186915 (11596)	130156 (13073)	127960 (10837)	183247 (15727)
Multiplicity	6.8 (6.3)	8.6 (5.6)	3.1 (3.2)	3.8 (1.9)	3.8 (2.2)
Completeness (%)	99.5 (98.3)	93.2 (57.9)	98.7 (99.8)	97.9 (83.5)	96.3 (83.0)
$\langle I/\sigma(I)\rangle$	13.5 (1.1)	21.1 (1.8)	6.6 (1.5)	4.9 (1.1)	7.2 (1.0)
Wilson B-factor ($Å^2$)	27.5	33.2	29.6	29.7	27.7
R_{merge}	0.069 (1.402)	0.061 (0.842)	0.134 (0.766)	0.191 (0.881)	0.132 (0.918)
R_{meas}	0.075 (1.527)	0.065 (0.928)	0.162 (0.923)	0.222 (1.113)	0.152 (1.190)
R_{pim}	0.028 (0.599)	0.021 (0.380)	0.089 (0.504)	0.110 (0.666)	0.074 (0.746)
$CC_{1/2}$	0.999 (0.600)	0.999 (0.795)	0.993 (0.620)	0.989 (0.537)	0.996 (0.508)
*CC**	1.000 (0.866)	1.000 (0.941)	0.998 (0.875)	0.997 (0.836)	0.999 (0.821)
Refinement statistics					
Working reflections	344004 (33867)	186869 (11591)	130007 (13069)	127827 (10835)	183007 (15708)
Test reflections	1032 (102)	1029 (64)	1040 (104)	1023 (87)	1007 (87)
R_{work}	0.138 (0.367)	0.147 (0.403)	0.179 (0.264)	0.180 (0.313)	0.180 (0.346)
R_{free}	0.159 (0.337)	0.162 (0.430)	0.225 (0.296)	0.227 (0.347)	0.222 (0.379)
CC_{work}	0.980 (0.797)	0.977 (0.883)	0.971 (0.814)	0.968 (0.731)	0.972 (0.709)
CC_{free}	0.982 (0.825)	0.980 (0.767)	0.943 (0.740)	0.937 (0.631)	0.960 (0.684)
Number of non-hydrogen atoms	16750	16326	16369	16088	16660
proteins	14392	14329	14312	14308	14317
ligands	324	332	315	315	358
solvent	2034	1665	1742	1465	1985
amino acid residues	1843	1843	1844	1843	1842
RMS_{bonds} (Å)	0.018	0.007	0.003	0.003	0.004
RMS_{angles} (°)	1.96	0.85	0.56	0.61	0.66
Ramachandran favored (%)	97.55	97.93	97.60	97.60	97.76
Ramachandran allowed (%)	2.34	1.91	2.40	2.34	2.18
Ramachandran outliers (%)	0.11	0.16	0.00	0.05	0.05
Rotamer outliers (%)	1.30	0.59	0.59	1.38	0.33
Clashscore	2.86	2.08	1.99	2.53	2.11
Average B-factor	33.42	39.05	37.18	37.31	33.97
macromolecules	31.94	38.17	36.65	36.98	32.78
ligands	32.90	37.04	34.95	34.22	35.72
solvent	44.02	46.97	41.96	41.24	42.22
Raw data deposition (DOI)	10.18150/UROCDW	10.18150/5AWAJZ	10.18150/K6NJZX	10.18150/CT5OD5	10.18150/AFE7CL
PDB code	7ZD1	7ZD0	7ZD2	7ZD4	7ZD3

* Statistics for the highest-resolution shell are shown in parentheses.

Table S4. Details on specific transition cation coordination by PASAHase with the corresponding cation-ligand distances (Å) listed for all chains (A-D).

Cation	Geometry	Chain/ion occupancy	C85 Sγ	D139 O	D139 Oδ1	H323 Nε	Wat1	Wat2	C59 Sγ	C59 O
Co^{2+}	Tetrahedral	A/0.45	2.31	2.11	2.41	2.22	-	-	-	-
		B/0.55	2.33	2.08	2.51	2.19	-	-	-	-
		C/0.45	2.39	2.17	2.48	2.16	-	-	-	-
		D/0.50	2.43	2.09	2.37	2.16	-	-	-	-
Zn^{2+}	Tetrahedral	A/1.00	2.28	2.10	1.96	2.27	-	-	-	-
		B/1.00	2.28	2.04	1.95	2.28	-	-	-	-
		C/1.00	2.26	2.08	1.94	2.27	-	-	-	-
		D/1.00	2.28	2.03	2.18	2.29	-	-	-	-
Cd^{2+}	Octahedral*	A/0.90	2.51	2.51	2.33	2.38	2.53	2.62	-	-
		B/0.85	2.61	2.50	2.47	2.43	2.59	2.65	-	-
		C/0.88	2.60	2.53	2.34	2.47	2.71	2.60	-	-
		D/0.80	2.60	2.49	2.38	2.44	2.69	-	-	-
$Hg^{2+}1$	Distorted** (four ligands)	A/0.25	2.32	2.65	3.11	1.92	-	-	-	-
		B/0.28	2.38	2.67	3.17	1.90	-	-	-	-
		C/0.27	2.37	2.84	3.04	1.98	-	-	-	-
		D/0.26	2.43	2.63	2.89	1.79	-	-	-	-
$Hg^{2+}2$	Distorted** (three ligands)	A/0.26	-	3.05	-	-	-	-	2.70	2.19
		B/0.30	-	3.01	-	-	-	-	2.80	2.23
		C/0.28	-	3.07	-	-	-	-	2.65	2.32
		D/0.42	-	2.98	-	-	-	-	2.76	1.94

* The octahedral coordination sphere of the Cd^{2+} cation is completed by two water molecules in chains A-C, whereas only one water molecule coordinates the cation in the subunit D.

** A significant disorder of the macromolecular environment that could not be satisfactorily resolved, as well as low occupancies of both Hg^{2+} ions, cause the coordination geometry, especially cation-ligand distances, cannot be determined with confidence.

Supplementary Figures

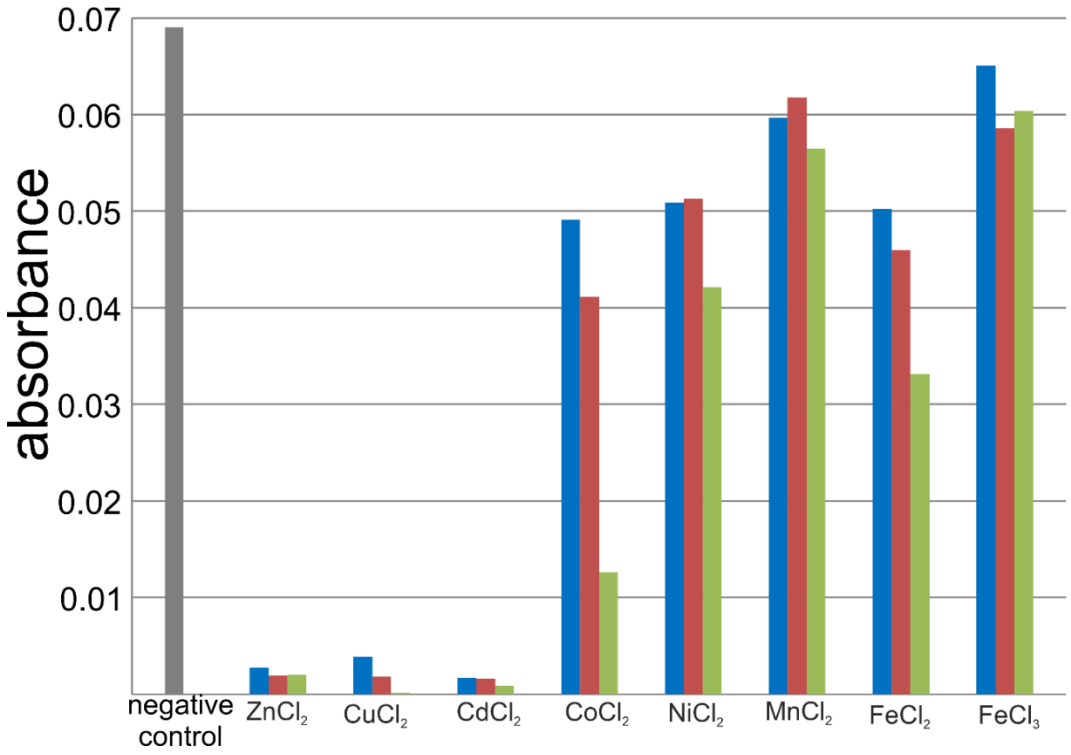

Figure S1. Initial study on inhibition of PaSAHase with some biologically and toxicologically relevant transition metal cations. Tests were conducted for the enzyme in the presence of Zn^{2+}, Cu^{2+}, Cd^{2+}, Co^{2+}, Ni^{2+}, Mn^{2+}, Fe^{2+} and Fe^{3+} ions. Tests were conducted at three cation concentrations corresponding to 1 (blue), 10 (red) and 100 μM (green bar). All measurements were performed at 293 K. Negative control was the enzymatic reaction without the addition of any transition metal cation.

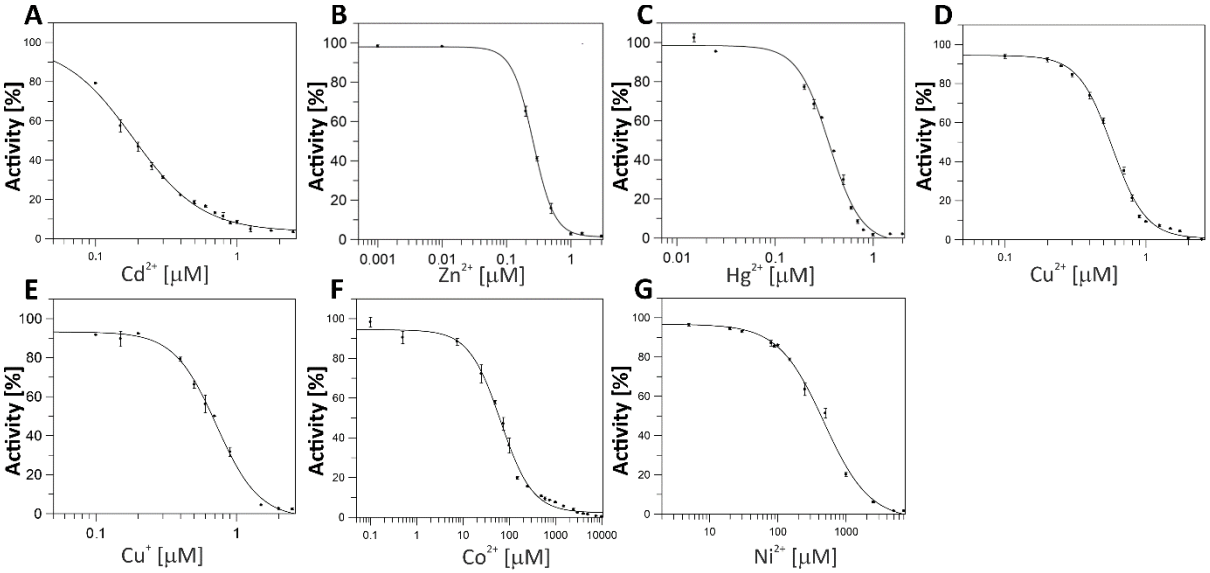

Figure S2. The influence of transition metal cations with PaSAHase. Enzyme inhibition studies were conducted for the enzyme in the presence of Cd^{2+}, Zn^{2+}, Hg^{2+}, Cu^{2+}, Cu^{+}, Co^{2+} and Ni^{2+} ions. Activities were measured at variable cations concentrations to determine the IC_{50} constants; all measurements were performed at 293 K in duplicates. Bars represent standard errors of the mean values.

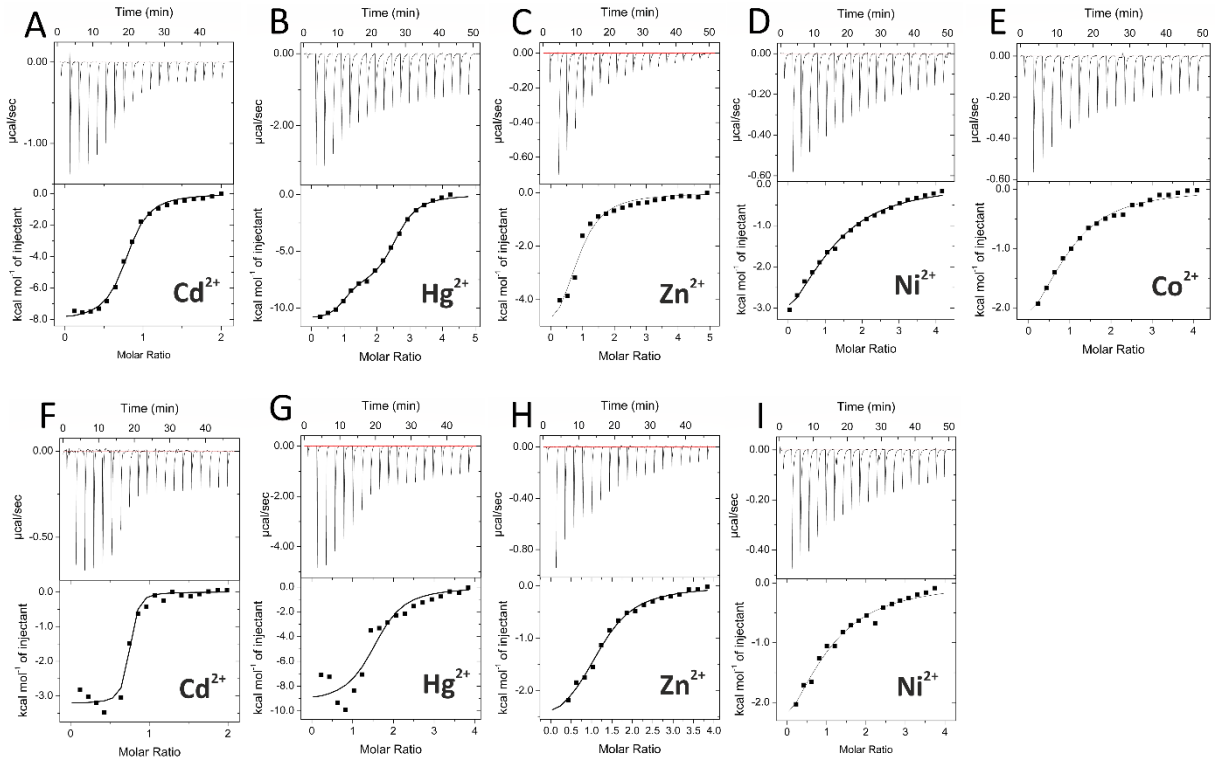

Figure S3. Representative raw data (upper panels) and integrated peaks with the best fit of one set of sites model (bottom panels) were obtained after titrations of PaSAHase with M^{2+} in the absence (A-E) or presence (F-I) of adenosine.

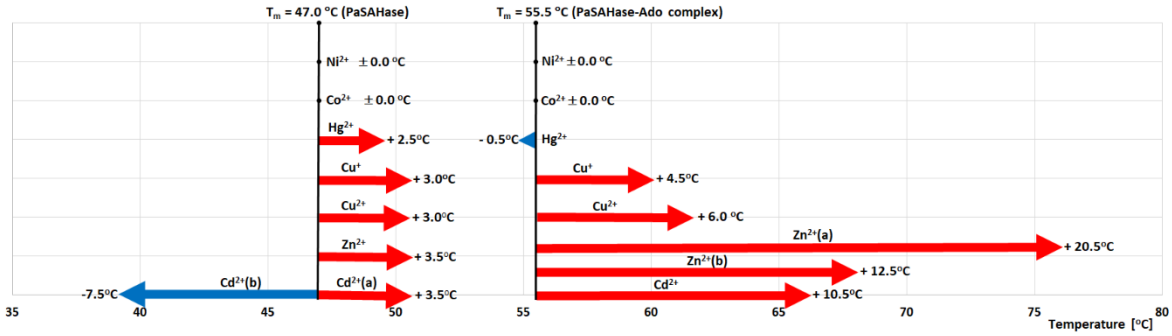

Figure S4. PaSAHase melting temperature shifts in the presence of transition metal cations. Red arrows correspond to an increase, whereas blue ones correspond to a weakened thermal stability estimated for the cations under investigation. Some ions affect individual domains separately, as double melting temperature shifts are observed for Cd^{2+} and Zn^{2+}. (A) Results presented for the open-form enzyme. (B) Results presented for the PaSAHase-Ado complex in the closed conformation.

Figures S5. Observed masses of the PaSAHase reaction products.

Reaction without addition of Cu^{2+} ions

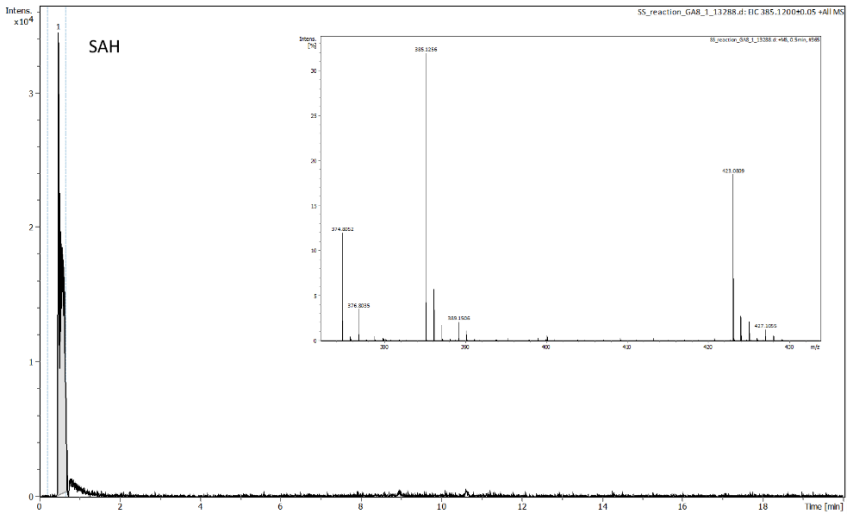

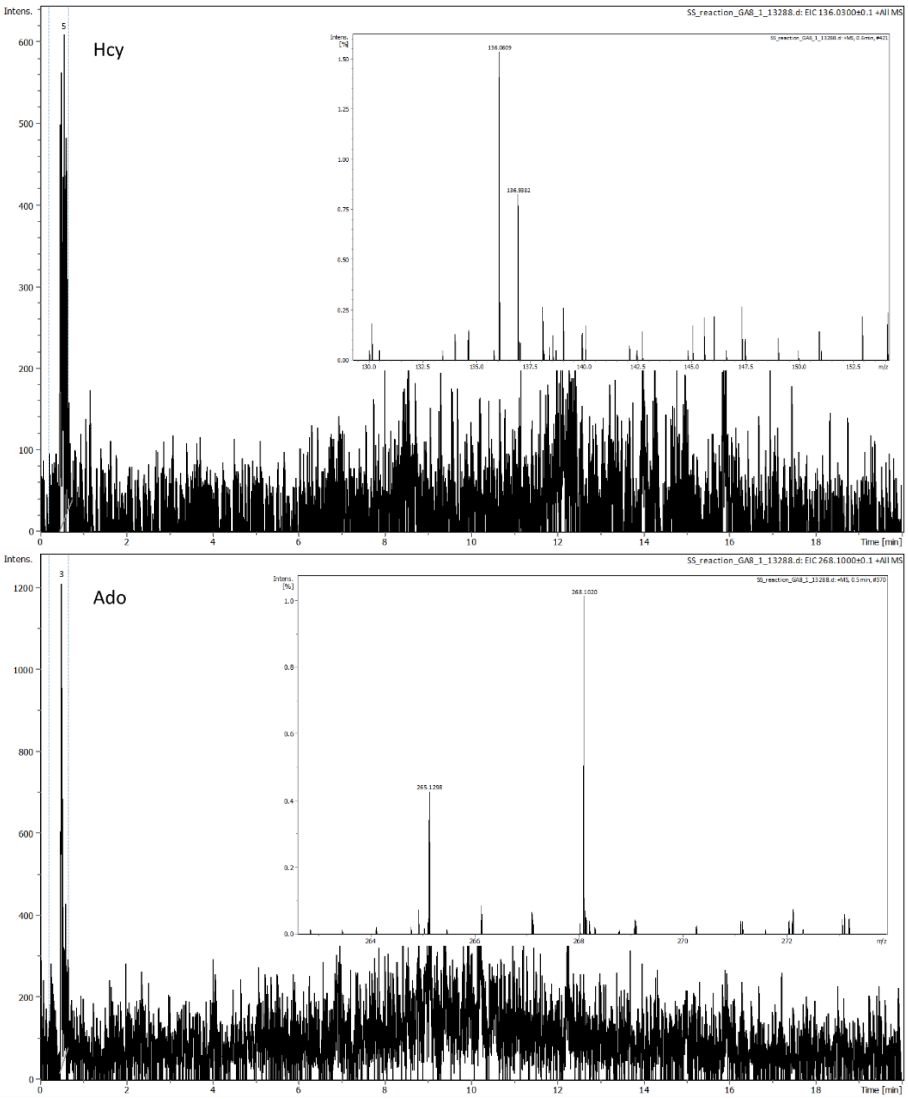

Reaction after the addition of Cu^{2+} ions

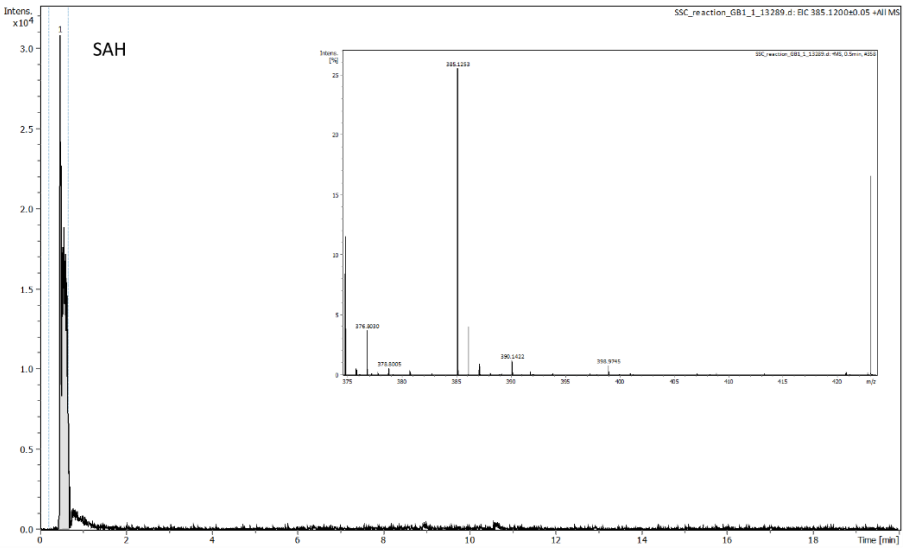

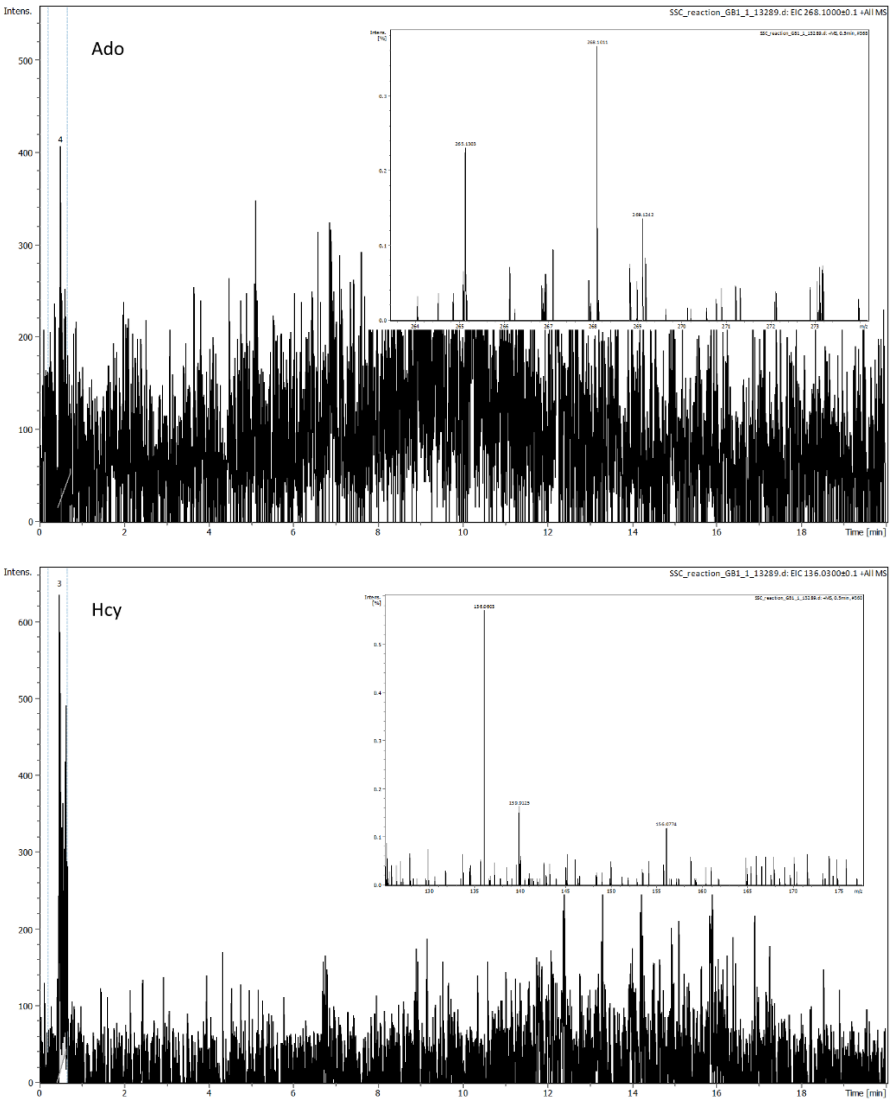
Intens.
SSC_reaction_GB1_1_13289.d: EIC 268.1000±0.1 +All MS
Ado
4
Time [min]
Intens.
SSC_reaction_GB1_1_13289.d: EIC 136.0300±0.1 +All MS
Hcy
3
Time [min]

References

1 J. Czyrko, J. Sliwiak, B. Imiolczyk, Z. Gdaniec, M. Jaskolski and K. Brzezinski, *Sci. Rep.*, 2018, **8**, 11334.
2 C. S. Yuan, J. Yeh, S. Liu and R. T. Borchardt, *J. Biol. Chem.*, 1993, **268**, 17030–17037.
3 R. Z. Cer, U. Mudunuri, R. Stephens and F. J. Lebeda, *Nucleic Acids Res.*, 2009, **37**, W441–W445.
4 L. Reinhard, H. Mayerhofer, A. Geerlof, J. Mueller-Dieckmann and M. S. Weiss, *Acta Crystallograph. Sect. F Struct. Biol. Cryst. Commun.*, 2013, **69**, 209–214.
5 M. Cianci, G. Bourenkov, G. Pompidor, I. Karpics, J. Kallio, I. Bento, M. Roessle, F. Cipriani, S. Fiedler and T. R. Schneider, *J. Synchrotron Radiat.*, 2017, **24**, 323–332.
6 W. Kabsch, *Acta Crystallogr. D Biol. Crystallogr.*, 2010, **66**, 125–132.
7 A. J. McCoy, R. W. Grosse-Kunstleve, P. D. Adams, M. D. Winn, L. C. Storoni and R. J. Read, *J. Appl. Crystallogr.*, 2007, **40**, 658–674.
8 J. Agirre, M. Atanasova, H. Bagdonas, C. B. Ballard, A. Baslé, J. Beilsten-Edmands, R. J. Borges, D. G. Brown, J. J. Burgos-Mármol, J. M. Berrisford, P. S. Bond, I. Caballero, L. Catapano, G. Chojnowski, A. G. Cook, K. D. Cowtan, T. I. Croll, J. É. Debreczeni, N. E. Devenish, E. J. Dodson, T. R. Drevon, P. Emsley, G. Evans, P. R. Evans, M. Fando, J. Foadi, L. Fuentes-Montero, E. F. Garman, M. Gerstel, R. J. Gildea, K. Hatti, M. L. Hekkelman, P. Heuser, S. W. Hoh, M. A. Hough, H. T. Jenkins, E. Jiménez, R. P. Joosten, R. M. Keegan, N. Keep, E. B. Krissinel, P. Kolenko, O. Kovalevskiy, V. S. Lamzin, D. M. Lawson, A. A. Lebedev, A. G. W. Leslie, B. Lohkamp, F. Long, M. Malý, A. J. McCoy, S. J. McNicholas, A. Medina, C. Millán, J. W. Murray, G. N. Murshudov, R. A. Nicholls, M. E. M. Noble, R. Oeffner, N. S. Pannu, J. M. Parkhurst, N. Pearce, J. Pereira, A. Perrakis, H. R. Powell, R. J. Read, D. J. Rigden, W. Rochira, M. Sammito, F. Sánchez Rodríguez, G. M. Sheldrick, K. L. Shelley, F. Simkovic, A. J. Simpkin, P. Skubak, E. Sobolev, R. A. Steiner, K. Stevenson, I. Tews, J. M. H. Thomas, A. Thorn, J. T. Valls, V. Uski, I. Usón, A. Vagin, S. Velankar, M. Vollmar, H. Walden, D. Waterman, K. S. Wilson, M. D. Winn, G. Winter, M. Wojdyr and K. Yamashita, *Acta Crystallogr. Sect. Struct. Biol.*, 2023, **79**, 449–461.
9 G. N. Murshudov, P. Skubák, A. A. Lebedev, N. S. Pannu, R. A. Steiner, R. A. Nicholls, M. D. Winn, F. Long and A. A. Vagin, *Acta Crystallogr. D Biol. Crystallogr.*, 2011, **67**, 355–367.
10 M. D. Winn, M. N. Isupov and G. N. Murshudov, *Acta Crystallogr. D Biol. Crystallogr.*, 2001, **57**, 122–133.
11 J. Painter and E. A. Merritt, *J. Appl. Crystallogr.*, 2006, **39**, 109–111.
12 J. Painter and E. A. Merritt, *Acta Crystallogr. D Biol. Crystallogr.*, 2006, **62**, 439–450.
13 P. Emsley, B. Lohkamp, W. G. Scott and K. Cowtan, *Acta Crystallogr. D Biol. Crystallogr.*, 2010, **66**, 486–501.
14 H. Berman, K. Henrick and H. Nakamura, *Nat. Struct. Biol.*, 2003, **10**, 980–980.